ACS Sustainable Chemistry & Engineering

Research Article

pubs.acs.org/journal/ascecg

One-Step Fabrication of Graphene Oxide Enhanced Magnetic Composite Gel for Highly Efficient Dye Adsorption and Catalysis

Zehong Cheng,[†] Jie Liao,[†] Benzhao He,[†] Fan Zhang,*[,‡] Faai Zhang,[†] Xiaohua Huang,[†] and Li Zhou*[,†]

[†]Guangxi Ministry-Province Jointly-Constructed Cultivation Base for State Key Laboratory of Processing for Nonferrous Metal and Featured Materials, Key Laboratory of New Processing Technology for Nonferrous Metal and Materials (Ministry of Education) and College of Material Science and Engineering, Guilin University of Technology, Guilin 541004, People's Republic of China

[‡]College of Chemistry and Chemical Engineering, Jishou University, Jishou 416000, People's Republic of China

Supporting Information

ABSTRACT: Graphene oxide (GO) is emerging as a potential adsorbent for environmental cleanup due to its attractive attributes associated with high removal efficiency toward water pollutants. However, it is difficult to separate GO from water after adsorption. Until now, the development of an effective approach that can simultaneously take advantage of the adsorption feature of GO and overcome the separation problem is still a challenge. Herein, we demonstrate a simple one-step approach to fabricate magnetic GO/poly(vinyl alcohol) (PVA) composite gels (mGO/PVA CGs), which not only exhibit convenient magnetic separation capability but also show remarkably enhanced adsorption capacity for cationic methylene blue (MB) and methyl violet (MV) dyes as compared with the one without GO (e.g., the adsorption capacities of mGO/PVA-50% and mGO/PVA-0% for MB are 231.12 and 85.64 mg/g, respectively). Detailed adsorption studies reveal that the adsorption kinetics and isotherms can be well-described by pseudo-second-order model and Langmuir isotherm model, respectively. Moreover, the adsorbent could be well regenerated in an acid solution without obvious compromise of removal efficiency. Considering the facile fabrication process and robust adsorption performance of the mGO/PVA CG, this work opens up enormous opportunities to bring GO from experimental research to practical water treatment applications. In addition, the mGO/PVA CG can act as a magnetic support for in situ growth of noble metal nanocatalyst with excellent catalytic performance, as exemplified by the synthesis of mGO/PVA-Pt catalyst in this paper.

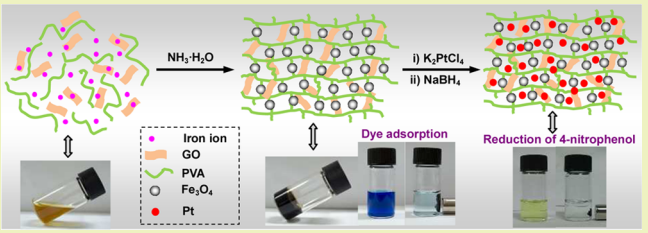

KEYWORDS: *Graphene oxide, Magnetic composite gel, Adsorption, Dye, Catalysis, Reduction of 4-nitrophenol*

INTRODUCTION

During the past decade, the development of advanced adsorbent materials for environmental cleanup has gained increasing attention.[1,2] Organic dye is one of the main water pollutants that can cause serious damage to human beings and aquatic biota by carcinogenic and mutagenic effects.[2−4] Various techniques including biological, chemical and physical techniques have been developed to remove dye from contaminated water.[3−7] Among them, the adsorption technique is particularly attractive due to its simplicity of design, ease of operation, high efficiency as well as the wide suitability for diverse dyes.[3−7] An ideal adsorbent is expected to show simultaneously a high adsorption capacity, rapid adsorption rate, high selectivity and facile separation process.

Graphene oxide (GO), a two-dimensional carbon nanomaterial, possesses ultralarge specific surface area, abundant oxygen-containing groups (e.g., −OH and −COOH) and excellent water dispersibility, which make it a nice adsorbent candidate for dye removal through the combination of electrostatic attraction, $\pi-\pi$ stacking and hydrogen bonding interactions between the GO and dye molecules.[8−10] In recent years, several groups have investigated the utilization of GO as an adsorbent to remove dyes from water and found that the GO exhibited ultrahigh adsorption capacity toward cationic dyes as compared with other adsorbents.[11−14] For instance, the adsorption capacity of GO for methylene blue (MB) dye, one of the most widely used cationic dyes, can reach as high as 714 mg/g.[11] However, it is hard to separate the highly water dispersible GO adsorbent from the dye solution after adsorption, and thus the practical application of GO as an adsorbent is seriously restricted. At the same time, the residual GO in aqueous solution may cause secondary pollution.

To overcome this drawback, hybridization of GO with other inorganic[15−17] or organic[18−22] materials such as sepiolite,[15] Ag/ZnO,[16] chitosan,[18] calcium alginate[19] and polypyrrole[20] has been investigated. Unfortunately, the obtained GO-based adsorbents still required a complex separation process. Recently, an effective protocol to facilitate the GO separation was developed by decorating GO surface with magnetic nanoparticles.[23−28] Benefiting from the magnetic characteristic,

Received: May 2, 2015
Revised: June 3, 2015
Published: June 15, 2015

DOI: 10.1021/acssuschemeng.5b00383
ACS Sustainable Chem. Eng. 2015, 3, 1677−1685

the magnetic GO can be readily collected from dye solution by a magnet after adsorption. However, the coverage of magnetic nanoparticles on the surface of GO hindered the direct contact between dye molecules and GO, resulting in significant decline of adsorption capacity (e.g., the adsorption capacity of magnetic GO for MB is 64.23 mg/g[26]). Therefore, exploring a simple and effective method to simultaneously take advantage of the merit of GO and solve the separation problem is still demanded.

To address the challenge, we present herein a one-step approach to prepare magnetic GO/poly(vinyl alcohol) (PVA) composite gel (mGO/PVA CG) based on the simultaneous formation of magnetic iron oxide nanoparticles (MIONs) and cross-linking of PVA and GO (Scheme 1). The utilization of mGO/PVA CG as a magnetic adsorbent to removal of cationic dyes from water was systematically investigated. Compared with the previous reports, the approach in this paper shows remarkably combined merits: (1) the mGO/PVA CG not only showed a strong magnetic property associated with the facile magnetic separation process but also exhibited a high adsorption capacity and selectivity toward cationic dyes; (2) the mGO/PVA CG can be synthesized in a large quantity without requirement of complex operation process, which is highly desired for practical applications. In addition, the mGO/PVA CG could also be employed as a magnetic support for in situ growth of noble metal nanocatalyst by first adsorption of metal ions through strong electrostatic interaction and then reduction of the adsorbed metal ions into corresponding metal nanoparticles, as exemplified by the in situ growth of Pt nanoparticles on mGO/PVA CG in this paper. The catalytic performance of the resulted mGO/PVA-Pt catalyst was also examined by the reduction of 4-nitrophenol.

Scheme 1. Schematic Illustration of the Synthetic Route to mGO/PVA CG

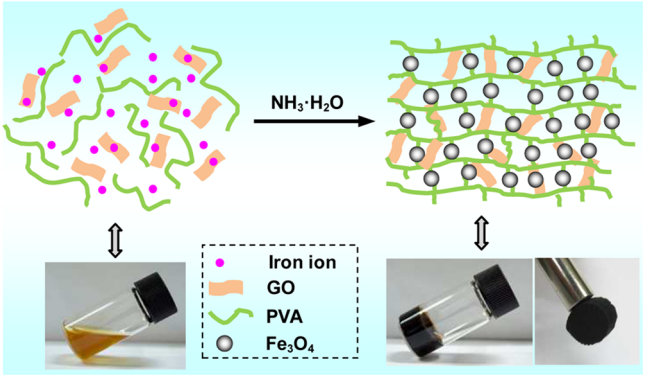

EXPERIMENTAL SECTION

Materials. Methylene blue (MB, λ_{max} = 662 nm), methyl orange (MO, λ_{max} = 463 nm), methyl violet (MV, λ_{max} = 583 nm), poly(vinyl alcohol) (Mw = 145 kDa), iron(II) chloride tetrahydrate ($FeCl_2 \cdot 4H_2O$), iron(III) chloride ($FeCl_3$) powder, ammonia solution (25 wt %), potassium tetrachloroplatinate (K_2PtCl_4), sodium borohydride ($NaBH_4$) and 4-nitrophenol (4-NP) were purchased from Aladdin Chemistry Co. Ltd. (Shanghai, China) and used as received. Graphene oxide (GO) nanosheets with thickness in the range of 0.75−0.80 nm (Figure S1 of the Supporting Information) were synthesized from graphite powder by a modified Hummer's method according to the literature.[29] All other chemicals were analytical grade and used as received without further purification. Milli-Q water (18.2 MΩ) was used throughout the experiments.

Characterization. Fourier transform infrared (FTIR) spectra were determined by a Thermo Nexus 470 FTIR spectrometer (KBr disk). Thermogravimetric analysis (TGA) was performed on a TGA Q500 analyzer under a nitrogen flow with a heating rate of 20 °C/min. Scanning electron microscopy (SEM) images were obtained using a FEISIRION 200 field-emission microscope. Transmission electron microscopy (TEM) and energy dispersive X-ray spectroscopy (EDS) studies were carried out on a JEOL-2010 TEM instrument at 160 kV. TEM microtome specimens were cut using a diamond knife. The samples of 90−100 nm thickness were collected on hexagonal 400 mesh copper grids. Atomic force microscopy (AFM) imaging of GO was conducted on a Digital Instrument Nanoscope IIIa scanning probe microscope, operating at the tapping mode. X-ray powder diffraction (XRD) spectra were collected on a Holland PANalytical X'Pert PRO X-ray diffractometer with Cu Kα radiation. The magnetic moment was determined on a MPMS XL-7 vibrating-sample magnetometer (VSM) at 300 K. UV−vis spectra were measured on a UV-3600 UV/vis spectrophotometer (Shimadzu).

Fabrication of Magnetic Graphene Oxide/Poly(vinyl alcohol) Composite Gel (mGO/PVA CG). Typically, PVA solution (45 mg/mL, 10 mL,), $FeCl_3$ solution (1 M, 2 mL) and $FeCl_2 \cdot 4H_2O$ solution (0.5 M, 2 mL) were added in a flask, and the mixture was stirred at room temperature for 20 min to dissolve the iron salt. After stoichiometric GO was added, the mixture was stirred for another 20 min. Subsequently, 20 mL of ammonia solution was added and black mGO/PVA CG was formed immediately. In addition, for preparation of bead-like mGO/PVA CG, the mixture of PVA, iron salt and GO was gradually dropped into 20 mL of ammonia solution by a dropper and black mGO/PVA gel beads with average diameter of 2 mm were formed immediately. Obviously, the size of the beads can be adjusted by manipulating the diameter of the dropper. After repeated washing by water, the final product was freeze-dried. To investigate the effect of GO content on the property of mGO/PVA CG, a series of products were fabricated through adjusting the weight feed ratios of GO to PVA from 5% to 50% by keeping other parameters as constant.

The swelling ratio of mGO/PVA CG was calculated as follows

$$\text{swelling ratio} = (W_s - W_d) \times 100\%/W_d \quad (1)$$

where W_d and W_s are the weight of dried mGO/PVA CG before and after immersing in water, respectively.

Dye Adsorption. The adsorption of dyes on mGO/PVA CG was conducted in a batch system. Typically, 20 mg of mGO/PVA CG was added in 5 mL of dye solution of known concentration and the mixture was agitated at 25 °C. The solution pH was adjusted with HCl (0.1 M) or NaOH (0.1 M). The samples were withdrawn from the flask at predetermined time intervals until the adsorption equilibrium was achieved. The adsorbent was separated from the dye solution by magnetic separation. All adsorption experiments were carried out in triplicate. Dye concentration was determined by UV−vis spectrophotometer. It should be pointed that the wavelength of absorption peaks of MB and MV solution at high pH (e.g., 9) or low pH (e.g., 3−4) are slightly changed as compared with those of solutions in the pH range 5−8. Calibration curves were plotted between absorbance and concentration of the standard dye solutions. The amount of dyes adsorbed at equilibrium was calculated from the following equation:

$$Q_e = \frac{(C_0 - C_e)V}{m} \quad (2)$$

where Q_e (mg/g) is the amount of dye adsorbed by mGO/PVA CG at equilibrium, C_0 and C_e are the initial and equilibrium concentrations of dye in the solution (mg/L) respectively, V is the volume of the solution (L) and m is the mass of mGO/PVA CG used (g).

Selective Adsorption of Cationic Dye from Dye Mixture. The selective adsorption experiments were performed in the mixture of MO and MB. Typically, 20 mg of mGO/PVA-50% was added to 5 mL of dye mixture. The initial concentrations of MB and MO are both 0.2 mM. After the mixture was stirred at 100 rpm/min for 0.5 h at room temperature, the mGO/PVA-50% was separated by a magnet. The

DOI: 10.1021/acssuschemeng.5b00383
ACS Sustainable Chem. Eng. 2015, 3, 1677−1685

residual dye concentration in the solution was determined by UV−vis spectrophotometry.

Synthesis of mGO/PVA-Pt Catalyst. Typically, 30 mg of mGO/PVA-50% was immersed in 5 mL of aqueous solution of K_2PtCl_4 (15 mM) for 24 h at room temperature. After that, the solid was separated by a magnet and washed with water repeatedly. Subsequently, the obtained solid was immersed in 5 mL of freshly prepared aqueous solution of $NaBH_4$ (0.05 M) and stirred for 30 min to afford the mGO/PVA-Pt catalyst.

Reduction of 4-Nitrophenol by mGO/PVA-Pt Catalyst. The reduction process was monitored by real-time UV−vis spectra. In a typical procedure, 4-nitrophenol (40 μL, 0.01 M), $NaBH_4$ (0.1 mL, 0.1 M) and water (2.5 mL) were added into a standard quartz cuvette. With the addition of 2 mg of mGO/PVA-Pt, the time-dependent absorption spectra were recorded. After the catalytic reaction, the mGO/PVA-Pt was collected by a magnet and washed with ethanol. To examine the reusability of mGO/PVA-Pt, the same catalytic procedure was repeated ten times.

RESULTS AND DISCUSSION

Synthesis and Characterization of mGO/PVA CG. The synthetic route to the mGO/PVA CG is depicted in Scheme 1, which employs only a one-step reaction. With the addition of an ammonia solution, the liquid mixture of PVA, GO and iron salt with light yellow color was gelled immediately to form black mGO/PVA CG. Benefiting from the facile synthetic process, it is able to fabricate mGO/PVA CG in a large quantity, which is highly desired for real applications. The synthetic protocol was designed based on the consideration of synergetic combination of coprecipitation, complexation and hydrogen bonding. On one hand, the GO and PVA can adsorb iron ions by their oxygen-containing functional groups in aqueous solution and subsequently act as a stabilizer to control the nucleation and growth of MIONs. On the other hand, the MIONs can not only endow GO and PVA with an excellent magnetic property but also act as a cross-linker to gelate the GO and PVA.[30] To investigate the effect of GO content on the property of mGO/PVA CG, a series of mGO/PVA CGs were prepared by adjusting the weight feed ratios of GO to PVA (f_{wt}) from 5% to 50%. It is worth noting that when the f_{wt} value is over 50%, the obtained mGO/PVA CG becomes very brittle with poor mechanical property. This is possibly caused by the fact that too high of GO content would lead to formation of mGO/PVA CG with a low degree of cross-linking. Moreover, to meet the requirement of practical application, mGO/PVA CG with diverse shapes could be readily achieved by tuning the shape of the reactor and the GO content based on the in situ gelation reaction (Figure 1). For example, film-like mGO/PVA CG can be prepared by adding ammonia solution onto the surface of a flat glass that contained the liquid mixture of GO, PVA and iron salt.

After further freezing-drying to remove water, the sponge-like mGO/PVA CGs were obtained. The internal morphologies of mGO/PVA CGs with different GO contents were observed by scanning electron microscopy (SEM), as presented in Figure 2. All the samples show a highly porous microstructure with a wide pore size distribution. Interestingly, the mean size of the pore can be adjusted in the range of 0.2−3 μm by manipulating the f_{wt} from 5% to 50%. The pores formed in the mGO/PVA-CGs are beneficial for transporting guest molecules and ions across the gel, thus providing a favorable platform for removal of pollutants from water.

To gain more insight into the structural and surface information on the mGO/PVA CG, mGO/PVA-50% as a representative was characterized by FTIR, X-ray diffraction (XRD), transmission electron microscopy (TEM) and vibrating-sample magnetometer (VSM) measurements. From the FTIR spectrum in Figure 3a, the mGO/PVA-50% sample exhibits a strong Fe−O vibration band at around 580 cm^{-1} due to the presence of MIONs.[7] In addition, the two obvious bands at 1720 and 3430 cm^{-1} confirms the presence of carboxylic and hydroxyl groups, respectively. The crystalline structure of mGO/PVA-50% was identified by powder XRD (Figure 3b). The two wide peaks appeared at 2θ of 10.8° and 19.7° are assigned to the characteristic peak of GO and PVA, respectively.[28,30] The characteristic peaks corresponding to magnetic Fe_3O_4 (JCPDS 19-0629) can also be clearly observed.[30] Seen from the representative TEM images of mGO/PVA-50% sample (Figure S2 of the Supporting Information), Fe_3O_4 nanoparticles with size in the range of 4−7 nm are uniformly distributed in the gel matrix. Owing to the presence of Fe_3O_4 nanoparticles, the mGO/PVA-50% sample shows a strong superparamagnetic property with a saturation magnetization value of 5.4 emu/g at 300 K (Figure 3c). The excellent magnetic performance of mGO/PVA-50% promises the facile magnetic separation for further applications. In addition, the swelling properties of mGO/PVA-CGs were determined, as depicted in Figure 3d. All the samples exhibit

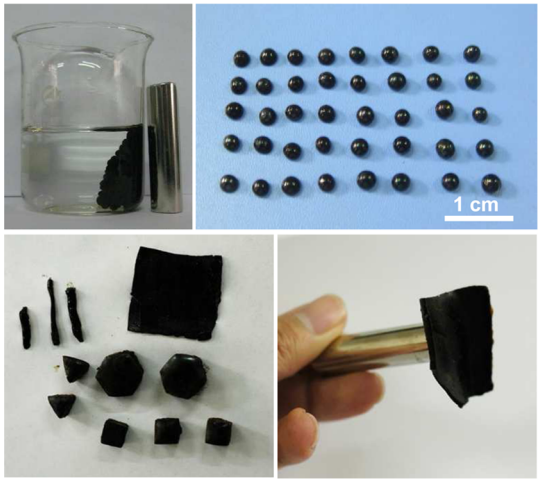

Figure 1. Photographs of mGO/PVA CG with diverse shapes.

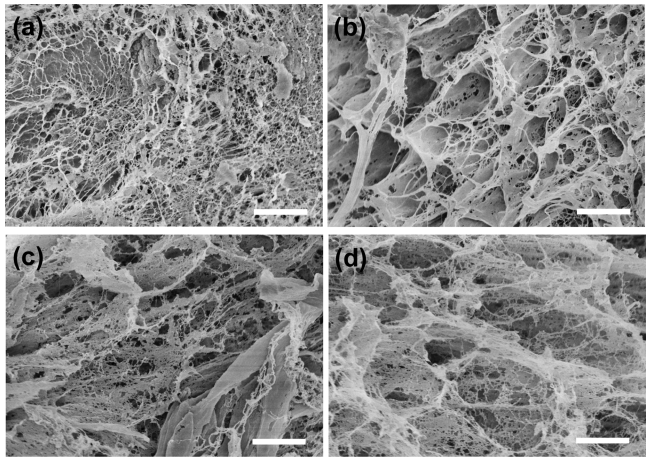

Figure 2. Representative SEM images of mGO/PVA-5% (a), mGO/PVA-15% (b), mGO/PVA-30% (c) and mGO/PVA-50% (d). The scale bar is 2 μm.

DOI: 10.1021/acssuschemeng.5b00383
ACS Sustainable Chem. Eng. 2015, 3, 1677−1685

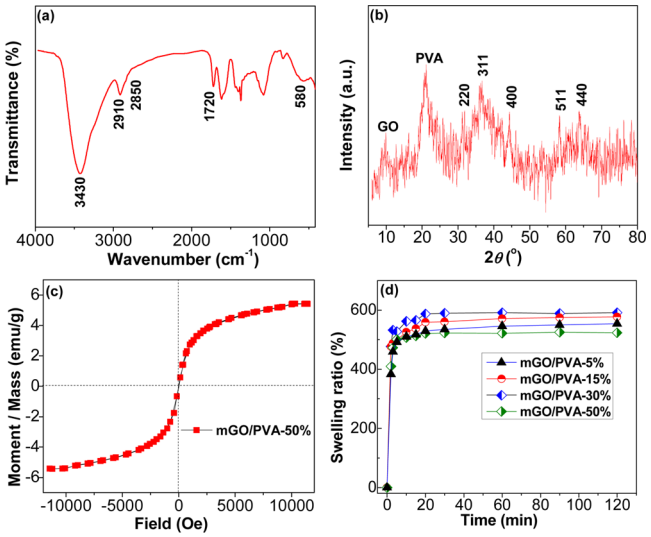

Figure 3. (a) FTIR spectrum, (b) XRD pattern and (c) magnetization curve (300 K) of mGO/PVA-50%. (d) Swelling ratio of mGO/PVA-5%, mGO/PVA-15%, mGO/PVA-30% and mGO/PVA-50%.

rapid swelling behavior and the swelling process can reach equilibrium within 30 min. There is no doubt that such a rapid swelling process can facilitate the fast adsorption of dyes from water. In addition, the mGO/PVA-50% sample shows a relatively low swelling ratio due to its low degree of cross-linking.

Dye Adsorption. For the batch dye adsorption experiments, bead-like mGO/PVA-CGs were studied as magnetic adsorbents. Methylene blue (MB) and methyl violet (MV), as two typical cationic dyes, were chosen to examine the adsorption performance of mGO/PVA-CGs. The chemical structures of MB and MV have rich cationic atoms (e.g., N^+) and aromatic rings (Figure 4a), which are favorable for uptake of GO surface through electrostatic and $\pi-\pi$ stacking interaction. At a relatively low initial concentration (0.1 mM), the MB and MV dyes could almost be completely removed from water by mGO/PVA-50% within 5 min, as exhibited in Figure 4b,c. Moreover, the adsorbent could be readily collected from the dye solution by a magnet. Because the adsorption capacity is considered as one of the most crucial parameters in practical application, the saturated adsorption capacities of mGO/PVA-CGs at a high initial dye concentration (4 mM) were determined (Figure 4d). Obviously, the introduction of GO can remarkably enhance the adsorption capacity of mGO/PVA-CGs. In particular, the saturated adsorption capacity of the mGO/PVA-50% sample for MB and MV dyes can respectively reach as high as 231.12 and 204.74 mg/g, which is much higher than that of mGO/PVA-0%. The enhancement of adsorption capacity is attributed to the presence of strong interactions such as electrostatic and $\pi-\pi$ stacking interactions between the GO component and dye molecules. In contrast, all the mGO/PVA CGs exhibited low adsorption capacities (<35 mg/g) for anionic methyl orange (MO) dye (Figure S3 of the Supporting Information); meanwhile, the adsorption capacity declined with increasing GO content. To understand further the adsorption process, the adsorption kinetics and isotherms were studied in detail by choosing mGO/PVA-50% as a representative.

The contact time required to reach equilibrium is an important parameter for dye removal. To establish the time

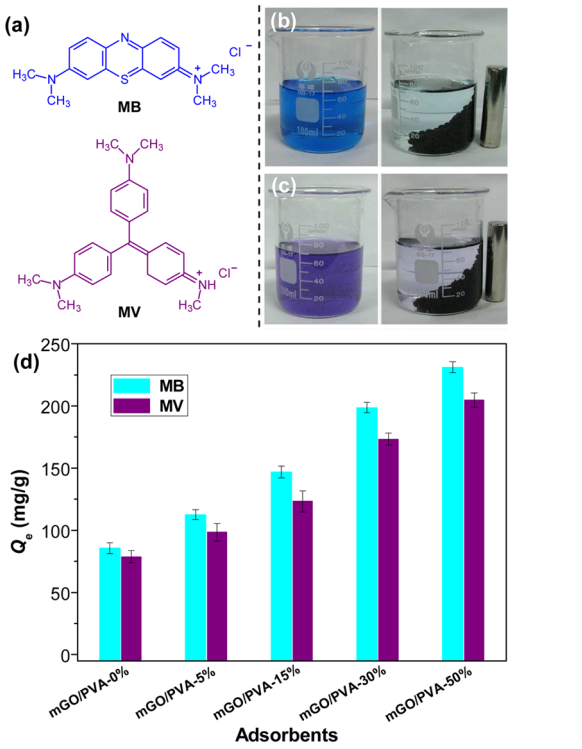

Figure 4. (a) Chemical structures of MB and MV. Photographs of MB (b) and MV (c) solutions (0.1 mM) before (left) and after (right) stirring with mGO/PVA-50% for 5 min. (d) Adsorption capacities of mGO/PVA-0%, mGO/PVA-5%, mGO/PVA-15%, mGO/PVA-30% and mGO/PVA-50%. The initial dye concentration is 4 mM.

dependence of adsorption, the adsorption capacities of mGO/PVA-50% for MB and MV solutions (0.5 mM) at diverse contact times were measured experimentally. As depicted in Figure 5a, the adsorption amounts for both MB and MV increased rapidly in the initial stage, and then slowed down until the adsorption process reached equilibrium in around 150 min. To our delight, over 85% of MB and MV could be removed within the first 60 min, indicated rapid adsorption rate of mGO/PVA-50% adsorbent. In addition, the adsorption data were analyzed by a well-known kinetic model, namely the pseudo-second-order model, as follows[31,32]

$$\text{pseudo-second-order equation: } \frac{t}{Q_t} = \left(\frac{1}{kQ_e^{\,2}}\right) + \frac{t}{Q_e} \quad (2)$$

where Q_t (mg/g) is the amount of dye adsorbed at the time t (min) and k (g mg^{-1} min^{-1}) is the pseudo-second-order rate constant. As shown in Figure 5b, two linear plots of t/Q_t against t give high correlation coefficients (R^2) of 0.9946 and 0.9958 for MB and MV, respectively. The high R^2 values suggest that the pseudo-second-order model is suitable for description of the dye adsorption process by mGO/PVA-50%. To study well the adsorption mechanism, the relationship between the amount of dye adsorbed and the dye remaining in solution is given in Figure 5c. The equilibrium adsorption data were analyzed by the famous Langmuir and Freundlich isotherm models (for details, see Table S1, Figure S4 and S5 in the Supporting Information).[30−34] The results in Table S1 of the Supporting Information reveal that the Langmuir model fits better than the Freundlich model to the adsorption data,

DOI: 10.1021/acssuschemeng.5b00383
ACS Sustainable Chem. Eng. 2015, 3, 1677−1685

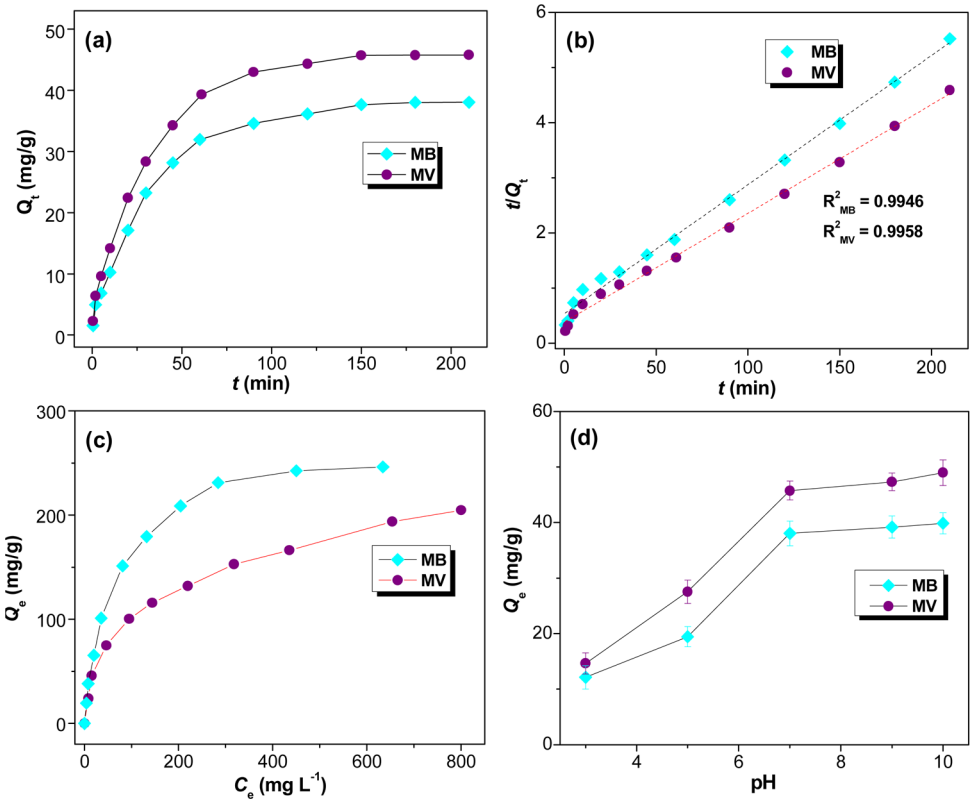

Figure 5. (a) Effect of contact time on the adsorption of MB and MV by mGO/PVA-50% adsorbent at pH 7.0 and 25 °C. The initial dye concentration is 0.5 mM. (b) Linear dependence of t/Q_t on t based on the pseudo-second-order model. (c) Adsorption isotherms for the adsorption of MB and MV on mGO/PVA-50% adsorbent at pH 7.0 and 25 °C. (d) Effect of pH on the adsorption of MB and MV by mGO/PVA-50% adsorbent at 25 °C.

suggesting that the main adsorption process obey monolayer coverage of dye onto the surface of mGO/PVA-50%. According to the Langmuir isotherm model, the maximum adsorption capacity (Q_{max}) value of mGO/PVA-50% for MB and MV can reach 270.94 and 221.23 mg/g, respectively. Because the adsorption of MB by other magnetic adsorbents has been widely reported, the Q_{max} value of mGO/PVA-50% for MB was compared with those of other magnetic adsorbents (see Table 1).[26−28,35−44] For comparison, we also synthesized magnetic GO according to the literature.[28] As the quality of GO synthesized by different conditions largely varied, the Q_{max} values of the prepared GO and magnetic GO for adsorption of MB were also determined (Figure S6 of the Supporting Information). The Q_{max} values of GO and magnetic GO according to the Langmuir isotherm are 657.89 and 188.32 mg/g, respectively. It can be seen from Table 1 that the Q_{max} value of mGO/PVA-50% is much higher than most of those reported for magnetic adsorbents such as magnetic GO (64.23−167.3 mg/g)[26−28] and magnetic graphene (45.27−73.26 mg/g).[35,36] In addition, the effect of the temperature on the adsorption performance of mGO/PVA-50% was studied. As depicted in Figure S7 of the Supporting Information, both the adsorption rate and adsorption capacity of the mGO/PVA-50% adsorbent were slightly enhanced with increasing temperature from 25 to 60 °C. On the basis of the above results, the mGO/PVA-50% can play a role as an excellent adsorbent not only for its facile magnetic separation characteristic but also for its efficient adsorption behavior on cationic aromatic dyes via strong $\pi-\pi$ stacking interaction and ionic interaction.[11−14]

Table 1. Comparison of the Maximum Monolayer Adsorption of MB onto Various Magnetic Adsorbents

adsorbent	Q_{max} (mg/g)	reference
magnetic GO	64.23	26
magnetic β-cyclodextrin/chitosan/GO	84.32	27
magnetic GO-Fe_3O_4 hybrid	167.3	28
magnetic Fe_3O_4−graphene composite	45.27	35
magnetic graphene@carbon hybrid	73.26	36
magnetic Fe_2O_3−carbon nanotube hybrid	42.3	37
magnetic carbon nanotube	15.74	38
magnetic Fe_3O_4@C	44.38	39
magnetic rectorite/Fe_3O_4 composites	60.24	40
polymer modified magnetic nanoparticles	128.7	41
magnetic alginate beads	223.8	42
carboxymethyl-β-cyclodextrin/Fe_3O_4 composite	277.8	43
magnetic adsorbent (Na-(CS/PAA)n/MPC)	305.8	44
magnetic GO	188.32	this study
mGO/PVA-CG	270.94	this study

As the solution pH can influence aqueous chemistry and surface binding sites of the adsorbent, the effect of initial pH on the adsorption performance of mGO/PVA-50% was studied from pH 3 to 10 at 25 °C, contact time of 3 h and initial dye concentration of 0.5 mM. Figure 5d shows the adsorption capacities of mGO/PVA-50% for MB and MV at diverse pH values. With decreasing the pH from 10 to 3, the adsorption capacities for both MB and MV gradually decline. This is attributed to the fact that the variation of pH can affect the ionization of the dyes and the surface charges of GO. The

DOI: 10.1021/acssuschemeng.5b00383
ACS Sustainable Chem. Eng. 2015, 3, 1677−1685

decrease of adsorption capacity at low pH values is possibly caused by the protons competition with dye molecules for the limited adsorption sites. At high pH values, the electrostatic attraction between the negatively charged surface of GO and cationic MB or MV molecule was enhanced, leading to an increase of dye uptake by mGO/PVA-50% adsorbent. On the basis of this phenomenon, the dye-adsorbed mGO/PVA-50% adsorbent may be able to desorb dye at low pH values. On the other hand, an excellent adsorbent should not only possess high adsorption capacity but also high reusability in order to reduce the overall cost of the adsorbent. Herein, the regeneration experiments were carried out by immersing dye-adsorbed mGO/PVA-50% in HCl solution (0.1 M) and then dialyzed for 24 h. After desorption, the regenerated mGO/PVA-50% was reused for the next adsorption, as presented in Figure 6. The

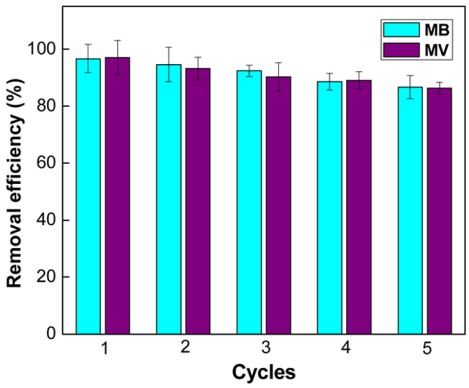

Figure 6. Removal efficiency of mGO/PVA-50% adsorbent in five successive cycles of desorption–adsorption compared with the original adsorption capacity.

results indicated that the removal efficiency reduced not more than 15%, even after five successive cycles of desorption–adsorption, as compared with the original adsorption capacity.

In addition, a nice adsorbent should be able to separate a certain dye from a dye mixture.[5,32] Given the negatively charged surface of GO, it is expected that the mGO/PVA-50% can selectively remove cationic dye from a dye mixture. In this paper, the selective adsorption of MB from the mixture solution of MO and MB was studied, as depicted in Figure 7. After the mGO/PVA-50% adsorbent was added, the color of the mixture solution of MO and MB gradually turned from dark green to light yellow (Figure 7c,d). To determine further the change of dye concentration, UV–vis spectra were used to trace the separation process (Figure 7e). After adsorption for 15 min, the intensity of peak at 662 nm associated with MB decreased remarkably whereas no obvious decrease at 463 nm corresponding to MO was observed, demonstrating the high selectivity of mGO/PVA-50% for the adsorption of MB dye. The high selectivity is possibly due to the fact that the electrostatic attraction between mGO/PVA-50% and MB is the main driving force for the adsorption process.

Catalysis. Magnetic noble metal nanocatalysts that combine excellent catalytic performance with facile magnetic separation capability are highly desired for catalysis applications.[45−47] Because the mGO/PVA-CG contains numerous oxygen-containing functional groups, it was expected that the mGO/PVA-CG could adsorb noble metal ions by strong electrostatic attraction and complexation. Subsequent in situ reduction by $NaBH_4$ yielded noble metal nanoparticles that were decorated

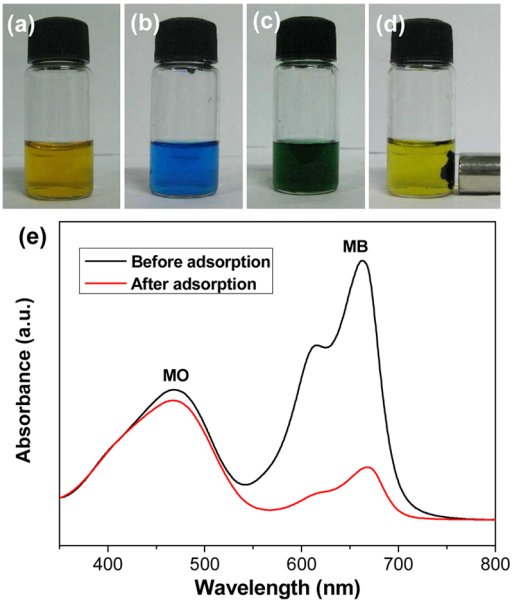

Figure 7. Photographs of aqueous solution of MO (a), MB (b) and mixture of MB and MO before (c) and after (d) adsorption on mGO/PVA-50%. (e) Absorption spectra of the mixed solution of MB and MO (0.1 mM) before and after adding mGO/PVA-50% for 15 min.

on the surface of mGO/PVA-CG. Herein, the mGO/PVA-50% sample was chosen as a representative for in situ growth of Pt nanoparticles, as illustrated in Scheme 2. The morphology of

Scheme 2. Schematic Illustration of the Synthetic Route to mGO/PVA-Pt

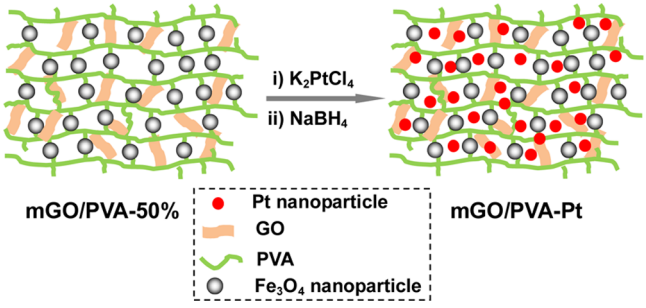

the resulted mGO/PVA-Pt hybrid was observed by TEM, as shown in Figure 8a,b. At low magnification, no big Pt aggregates are observed, indicating the good distribution of Pt nanoparticles on the surface of mGO/PVA-50%. Because the gel sample is too thick, it is difficult to distinguish the Pt nanoparticles and MIONs by lattice fringe, even at high magnification. However, all the nanoparticles exhibit a relatively uniform size distribution with sizes in the range of 5−10 nm, suggesting that the mGO/PVA-50% can serve as an efficient magnetic support for in situ growth of noble metal nanoparticles. The content of Pt according to the energy dispersive X-ray spectroscopy (EDS) result was about 0.254 mmol/g (Figure 8c), which is similar to the value (0.247 mmol/g) measured by inductively coupled plasma mass spectrometry (ICP-MS, Agilent 7500cx). In addition, the mGO/PVA-Pt hybrid still presented a strong superparamagnetic property and could be readily separated from water through a magnet (Figure 8d and Figure S8 of the Supporting Information).

DOI: 10.1021/acssuschemeng.5b00383
ACS Sustainable Chem. Eng. 2015, 3, 1677−1685

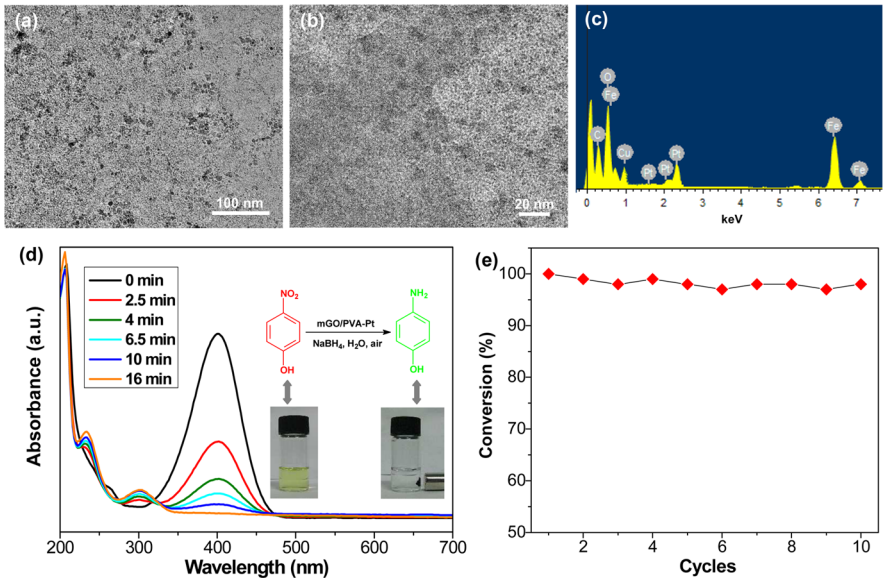

Figure 8. Representative TEM images of mGO/PVA-Pt at low (a) and high (b) magnifications. (c) EDS spectrum of mGO/PVA-Pt shown in panel b. (d) UV−vis spectra showing the gradual reduction of 4-NP with mGO/PVA-Pt catalyst. Inset: photographs of 4-NP and $NaBH_4$ solution before (left) and after (right) adding mGO/PVA-Pt. (e) Conversion of 4-NP in ten successive cycles of reduction and magnetic separation with mGO/PVA-Pt catalyst.

The catalytic activity of mGO/PVA-Pt was evaluated by using the catalytic reduction of 4-nitrophenol (4-NP) into 4-aminophenol. This reaction has been extensively used to evaluate the catalytic performance of noble metal catalysts.[42−47] On the other hand, the 4-NP is a commonly used chemical intermediate with high toxicity, and thus the elimination of 4-NP from industrial wastewater is essential. To exclude the influence of the concentration of $NaBH_4$ on the reduction rate, excess $NaBH_4$ was added as compared with 4-nitrophenol. The reduction process was monitored by recording the intensity of the absorption peak at 400 nm associated with 4-NP as a function of time (Figure 8d). Upon addition of the mGO/PVA-Pt catalyst, the peak at 400 nm gradually decreases; meanwhile, a new peak at 295 nm appears due to the formation of 4-aminophenol. The reduction reaction could also be observed by naked eyes because the 4-NP solution with bright yellow color gradually faded out during the reaction process (Figure 8d). Because the concentration of $NaBH_4$ is much higher than that of 4-nitrophenol, the pseudo-first-order kinetic model can be applied to evaluate the rate constant.[46−49] The kinetic equation can be expressed as

$$\ln(C'_t/C'_0) = -k_{ap}t' \quad (3)$$

where C'_0 (mM) is the initial concentration of 4-NP, C'_t (mM) is the concentration of 4-nitrophenol at time t' (s) and k_{ap} is the apparent rate constant. As shown in Figure S9b of the Supporting Informaiton, the plot of ln (C'_t/C'_0) against t' gives a straight line, indicating the good consistency with the pseudo-first-order kinetic model. In addition, the k_{ap} was calculated to be 3.59×10^{-3} s^{-1}, which compares favorably to other reported Pt-based catalysts.[49,50] Moreover, the mGO/PVA-Pt could be easily collected by a magnet and reused for at least ten successive cycles of reaction without decline of catalytic efficiency (Figure 8e). The high catalytic stability of mGO/PVA-Pt is attributed to the strong interfacial interactions between the Pt nanoparticles and the oxygen-containing functional groups of the mGO/PVA-50%. It is postulated that this approach can be extended to decorate mGO/PVA CGs with other noble metal nanoparticles to meet diverse requirements.

CONCLUSIONS

In summary, we have demonstrated an easy and effective approach to combine the adsorption feature of GO with convenient magnetic separation capability of magnetic gel based on the one-step fabrication of mGO/PVA CG. The obtained mGO/PVA CG not only exhibited strong super-paramagnetic property but also showed obvious GO content-dependent enhancement of adsorption capacity for cationic MB and MV dyes. The adsorption kinetics and isotherms studies demonstrated that the adsorption process can be well fitted by the pseudo-second-order kinetics and Langmuir isotherm model, respectively. In addition, the mGO/PVA CG can serve as a magnetic support for in situ growth of a noble metal nanocatalyst with high catalytic efficiency, as exemplified by the preparation of mGO/PVA-Pt catalyst in this paper. Moreover, the mGO/PVA CG showed fine reusability both for adsorption and catalysis applications. The finding in this paper clearly highlights the combined merits of GO and magnetic gel, consequently offering an effective strategy to fabricate versatile composites for various applications such as environmental treatment and catalysis. It is postulated that this study will gain intensive attention for both fundamental research and technological application not only due to the simple fabrication process but also due to the versatile performance of the product.

ASSOCIATED CONTENT

Supporting Information

AFM image of GO, TEM images of mGO/PVA-50%, adsorption capacities of mGO/PVA CGs for MO, detailed adsorption isotherm studies, adsorption isotherm of GO and magnetic GO for adsorption of MB, effect of temperature on the adsorption rate and adsorption capacity of mGO/PVA-

DOI: 10.1021/acssuschemeng.5b00383
ACS Sustainable Chem. Eng. 2015, 3, 1677−1685

50%, plot of $\ln(C'_t/C'_0)$ against time for the reduction of 4-nitrophenol with mGO/PVA-Pt catalysts. The Supporting Information is available free of charge on the ACS Publications website at DOI: 10.1021/acssuschemeng.5b00383.

AUTHOR INFORMATION

Corresponding Authors

*L. Zhou. E-mail: zhouli@glut.edu.cn.

*F. Zhang. E-mail: zhangfan8346@sina.com.

Notes

The authors declare no competing financial interest.

ACKNOWLEDGMENTS

The authors appreciate financial support from the National Natural Science Foundation of China (Grant No. 21364003), Key Science and Technology Financing Projects of Ministry of Education (Grant No. 211124) of China, Guangxi Natural Science Foundation (Grant No. 2014GXNSFCA118004), China Postdoctoral Science Foundation (Grant No. 2012M521559) and project of outstanding young teachers' training in higher education institutions of Guangxi.

REFERENCES

(1) Crini, G. Non-conventional low-cost adsorbents for dye removal: A review. *Bioresour. Technol.* **2006**, *97*, 1061−1085.

(2) Crini, G.; Badot, P. M. Application of chitosan, a natural aminopolysaccharide, for dye removal from aqueous solutions by adsorption processes using batch studies: A review of recent literature. *Prog. Polym. Sci.* **2008**, *33*, 399−447.

(3) Mondal, T.; Bhowmick, A. K.; Krishnamoorti, R. Synthesis and characterization of bi-functionalized graphene and expanded graphite using *n*-butyl lithium and their use for efficient water soluble dye adsorption. *J. Mater. Chem. A* **2013**, *1*, 8144−8153.

(4) Yang, Y.; Liao, H.; Tong, Z.; Wang, C. Porous Ag/polymer composite microspheres for adsorption and catalytic degradation of organic dyes in aqueous solutions. *Compos. Sci. Technol.* **2015**, *107*, 137−144.

(5) Deng, S.; Xu, H.; Jiang, X.; Yin, J. Poly(vinyl alcohol) (PVA)-enhanced hybrid hydrogels of hyperbranched poly(ether amine) (hPEA) for selective adsorption and separation of dyes. *Macromolecules* **2013**, *46*, 2399−2406.

(6) Liu, L.; Gao, Z. Y.; Su, X. P.; Chen, X.; Jiang, L.; Yao, J. M. Adsorption removal of dyes from single and binary solutions using a cellulose-based bioadsorbent. *ACS Sustainable Chem. Eng.* **2015**, *3*, 432−442.

(7) Zhou, L.; He, B.; Huang, J. One-step synthesis of robust amine- and vinyl-capped magnetic iron oxide nanoparticles for polymer grafting, dye adsorption, and catalysis. *ACS Appl. Mater. Interfaces* **2013**, *5*, 8678−8685.

(8) Dreyer, D. R.; Park, S.; Bielawski, C. W.; Ruoff, R. S. The chemistry of graphene oxide. *Chem. Soc. Rev.* **2010**, *39*, 228−240.

(9) Dikin, D. A.; Stankovich, S.; Zimney, E. J.; Piner, R. D.; Dommett, G. H.; Evmenenko, G.; Nguyen, S. T.; Ruoff, R. S. Preparation and characterization of graphene oxide paper. *Nature* **2007**, *448*, 457−460.

(10) Dong, Z.; Wang, D.; Liu, X.; Pei, X.; Chen, L.; Jin. Bio-inspired surface-functionalization of graphene oxide for the adsorption of organic dyes and heavy metal ions with a superhigh capacity. *J. Mater. Chem. A* **2014**, *2*, 5034−5040.

(11) Yang, S. T.; Chen, S.; Chang, Y.; Cao, A.; Liu, Y.; Wang, H. Removal of methylene blue from aqueous solution by graphene oxide. *J. Colloid Interface Sci.* **2011**, *359*, 24−29.

(12) Yu, Y.; Murthy, B. N.; Shapter, J. G.; Constantopoulos, K. T.; Voelcker, N. H.; Ellis, A. V. Benzene carboxylic acid derivatized graphene oxide nanosheets on natural zeolites as effective adsorbents for cationic dye removal. *J. Hazard. Mater.* **2013**, *260*, 330−338.

(13) Liu, F.; Chung, S.; Oh, G.; Seo, T. S. Three-dimensional graphene oxide nanostructure for fast and efficient water-soluble dye removal. *ACS Appl. Mater. Interfaces* **2012**, *4*, 922−927.

(14) Sharma, P.; Das, M. R. Removal of a cationic dye from aqueous solution using graphene oxide nanosheets: Investigation of adsorption parameters. *J. Chem. Eng. Data* **2012**, *58*, 151−158.

(15) Cheng, H.; Zeng, K.; Yu, J. Adsorption of uranium from aqueous solution by graphene oxide nanosheets supported onsepiolite. *J. Radioanal. Nucl. Chem.* **2013**, *298*, 599−603.

(16) Qin, J.; Li, R.; Lu, C.; Jiang, Y.; Tang, H.; Yang, X. Ag/ZnO/graphene oxide heterostructure for the removal of rhodamine B by the synergistic adsorption−degradation effects. *Ceram. Int.* **2014**, *41*, 4231−4237.

(17) Du, Q.; Sun, J.; Li, Y.; Yang, X.; Wang, X.; Wang, Z.; Xia, L. Highly enhanced adsorption of congo red onto graphene oxide/chitosan fibers by wet-chemical etching off silica nanoparticles. *Chem. Eng. J.* **2014**, *245*, 99−106.

(18) Yang, S. T.; Luo, J.; Liu, J. H.; Zhou, Q.; Wan, J.; Ma, C.; Liao, R.; Wang, H.; Liu, Y. Graphene oxide/chitosan composite for methylene blue adsorption. *Nanosci. Nanotechnol. Lett.* **2013**, *5*, 372−376.

(19) Li, Y.; Du, Q.; Liu, T.; Sun, J.; Wang, Y.; Wu, S.; Wang, Z.; Xia, Y.; Xia, L. Methylene blue adsorption on graphene oxide/calcium alginate composites. *Carbohydr. Polym.* **2013**, *95*, 501−507.

(20) Hu, R.; Dai, S.; Shao, D.; Alsaedi, A.; Ahmad, B.; Wang, X. Efficient removal of phenol and aniline from aqueous solutions using graphene oxide/polypyrrole composites. *J. Mol. Liq.* **2015**, *203*, 80−89.

(21) Zhang, C.; Wu, L.; Cai, D.; Zhang, C.; Wang, N.; Zhang, J.; Wu, Z. Adsorption of polycyclic aromatic hydrocarbons (fluoranthene and anthracenemethanol) by functional graphene oxide and removal by pH and temperature-sensitive coagulation. *ACS Appl. Mater. Interfaces* **2013**, *5*, 4783−4790.

(22) Wu, Z.; Zhong, H.; Yuan, X.; Wang, H.; Wang, L.; Chen, X.; Zeng, G.; Wu, Y. Adsorptive removal of methylene blue by rhamnolipid-functionalized graphene oxide from wastewater. *Water Res.* **2014**, *67*, 330−344.

(23) Geng, Z.; Lin, Y.; Yu, X.; Shen, Q.; Ma, L.; Li, Z.; Pan, N.; Wang, X. Highly efficient dye adsorption and removal: A functional hybrid of reduced graphene oxide−Fe_3O_4 nanoparticles as an easily regenerative adsorbent. *J. Mater. Chem.* **2012**, *22*, 3527−3535.

(24) Fan, L.; Luo, C.; Sun, M.; Li, X.; Lu, F.; Qiu, H. Preparation of novel magnetic chitosan/graphene oxide composite as effective adsorbents toward methylene blue. *Bioresour. Technol.* **2012**, *114*, 703−706.

(25) Shi, H.; Li, W.; Zhong, L.; Xu, C. Methylene blue adsorption from aqueous solution by magnetic cellulose/graphene oxide composite: Equilibrium, kinetics, and thermodynamics. *Ind. Eng. Chem. Res.* **2014**, *53*, 1108−1118.

(26) Deng, J. H.; Zhang, X. R.; Zeng, G. M.; Gong, J. L.; Niu, Q. Y.; Liang, J. Simultaneous removal of Cd(II) and ionic dyes from aqueous solution using magnetic graphene oxide nanocomposite as an adsorbent. *Chem. Eng. J.* **2013**, *226*, 189−200.

(27) Fan, L.; Luo, C.; Sun, M.; Qiu, H.; Li, X. Synthesis of magnetic *β*-cyclodextrin−chitosan/graphene oxide as nanoadsorbent and its application in dye adsorption and removal. *Colloids Surf., B* **2013**, *103*, 601−607.

(28) Xie, G.; Xi, P.; Liu, H.; Chen, F.; Huang, L.; Shi, Y.; Hou, F.; Zeng, Z.; Shao, C.; Wang, J. A facile chemical method to produce superpara- magnetic graphene oxide-Fe_3O_4 hybrid composite and its application in the removal of dyes from aqueous solution. *J. Mater. Chem.* **2012**, *22*, 1033−1039.

(29) He, H.; Gao, C. General approach to individually dispersed, highly soluble, and conductive graphene nanosheets functionalized by nitrene chemistry. *Chem. Mater.* **2010**, *22*, 5054−5064.

(30) Zhou, L.; He, B.; Zhang, F. Facile one-pot synthesis of iron oxide nanoparticles cross-linked magnetic poly(vinyl alcohol) gel beads for drug delivery. *ACS Appl. Mater. Interfaces* **2011**, *4*, 192−199.

(31) Zhang, X.; Liu, J.; Kelly, S. J.; Huang, X.; Liu, J. Biomimetic snowflake-shaped magnetic micro-/nanostructures for highly efficient

DOI: 10.1021/acssuschemeng.5b00383
ACS Sustainable Chem. Eng. 2015, 3, 1677−1685

adsorption of heavy metal ions and organic pollutants from aqueous solution. *J. Mater. Chem. A* **2014**, *2*, 11759−11767.
(32) Deng, S.; Wang, R.; Xu, H.; Jiang, X.; Yin, J. Hybrid hydrogels of hyperbranched poly(ether amine)s (hPEAs) for selective adsorption of guest molecules and separation of dyes. *J. Mater. Chem.* **2012**, *22*, 10055−10061.
(33) Miranda, L. D.; Bellato, C. R.; Fontes, M. P.; de Almeida, M. F.; Milagres, J. L.; Minim, L. A. Preparation and evaluation of hydrotalcite-iron oxide magnetic organocomposite intercalated with surfactants for cationic methylene blue dye removal. *Chem. Eng. J.* **2014**, *254*, 88−97.
(34) Zhou, L.; Gao, C.; Xu, W. Magnetic dendritic materials for highly efficient adsorption of dyes and drugs. *ACS Appl. Mater. Interfaces* **2010**, *2*, 1483−1491.
(35) Yao, Y.; Miao, S.; Liu, S.; Ma, L. P.; Sun, H.; Wang, S. Synthesis, characterization, and adsorption properties of magnetic Fe_3O_4@graphene nanocomposite. *Chem. Eng. J.* **2012**, *184*, 326−332.
(36) Fan, W.; Gao, W.; Zhang, C.; Tjiu, W. W.; Pan, J.; Liu, T. Hybridization of graphene sheets and carbon-coated Fe_3O_4 nanoparticles as a synergistic adsorbent of organic dyes. *J. Mater. Chem.* **2012**, *22*, 25108−25115.
(37) Qu, S.; Huang, F.; Yu, S.; Chen, G.; Kong, J. Magnetic removal of dyes from aqueous solution using multi-walled carbon nanotubes filled with Fe_2O_3 particles. *J. Hazard. Mater.* **2008**, *160*, 643−647.
(38) Gong, J. L.; Wang, B.; Zeng, G. M.; Yang, C. P.; Niu, C. G.; Niu, Q. Y.; Zhou, W. J.; Liang, Y. Removal of cationic dyes from aqueous solution using magnetic multi-wall carbon nanotube nanocomposite as adsorbent. *J. Hazard. Mater.* **2009**, *164*, 1517−1522.
(39) Zhang, Z.; Kong, J. Novel magnetic Fe_3O_4@C nanoparticles as adsorbents for removal of organic dyes from aqueous solution. *J. Hazard. Mater.* **2011**, *193*, 325−329.
(40) Wu, D.; Zheng, P.; Chang, P. R.; Ma, X. Preparation and characterization of magnetic rectorite/iron oxide nanocomposites and its application for the removal of the dyes. *Chem. Eng. J.* **2011**, *174*, 489−494.
(41) Ge, F.; Ye, H.; Li, M. M.; Zhao, B. X. Efficient removal of cationic dyes from aqueous solution by polymer-modified magnetic nanoparticles. *Chem. Eng. J.* **2012**, *198*, 11−17.
(42) Rocher, J.; Bee, A.; Siaugue, J. M.; Cabuil, V. Dye removal from aqueous solution by magnetic alginate beads crosslinked with epichlorohydrin. *J. Hazard. Mater.* **2010**, *178*, 434−439.
(43) Badruddoza, A. Z. M.; Hazel, G. S. S.; Hidajat, K.; Uddin, M. S. Synthesis of carboxymethyl-*β*-cyclodextrin conjugated magnetic nanoadsorbent for removal of methylene blue. *Colloids Surf., A* **2010**, *367*, 85−95.
(44) Chen, Y.; He, F.; Ren, Y.; Peng, H.; Huang, K. Fabrication of chitosan/PAA multilayer onto magnetic microspheres by LbL method for removal of dyes. *Chem. Eng. J.* **2014**, *249*, 79−92.
(45) Ge, J.; Huynh, T.; Hu, Y.; Yin, Y. Hierarchical magnetite/silica nanoassemblies as magnetically recoverable catalyst-supports. *Nano Lett.* **2008**, *8*, 931−934.
(46) Hoseini, S. J.; Rashidi, M.; Bahrami, M. Platinum nanostructures at the liquid−liquid interface: catalyticreduction of *p*-nitrophenol to *p*-aminophenol. *J. Mater. Chem.* **2011**, *21*, 16170−16176.
(47) Zhou, L.; Gao, C.; Xu, W. Robust Fe_3O_4/SiO_2-Pt/Au/Pd magnetic nanocatalysts with multifunctional hyperbranched polyglycerol amplifiers. *Langmuir* **2010**, *26*, 11217−11225.
(48) Cheng, Z.; He, B.; Zhou, L. A general one-step approach for in situ decoration of MoS_2 nanosheets with inorganic nanoparticles. *J. Mater. Chem. A* **2015**, *3*, 1042−1048.
(49) Ghosh, S. K.; Mandal, M.; Kundu, S.; Nath, S.; Pal, T. Bimetallic Pt−Ni nanoparticles can catalyze reduction of aromatic nitrocompounds by sodium borohydride in aqueous solution. *Appl. Catal., A* **2004**, *268*, 61−66.
(50) Li, H.; Jo, J. K.; Zhang, L.; Ha, C. S.; Suh, H.; Kim, I. A general and efficient route to fabricate carbon nanotube-metal nanoparticles and carbon nanotube-inorganic oxides hybrids. *Adv. Funct. Mater.* **2010**, *20*, 3864−3873.

DOI: 10.1021/acssuschemeng.5b00383
ACS Sustainable Chem. Eng. 2015, 3, 1677−1685